

# 3D quaternionic condensation and spin textures with Hopf invariants from synthetic spin-orbit coupling

Yi Li,<sup>1</sup> Xiangfa Zhou,<sup>2</sup> and Congjun Wu<sup>1</sup>

<sup>1</sup>*Department of Physics, University of California, San Diego, CA 92093, USA*

<sup>2</sup>*Key Laboratory of Quantum Information, University of Science and Technology of China, CAS, Hefei, Anhui 230026, China*

We study unconventional condensations of two-component bosons in a harmonic trap subject to the 3D  $\vec{\sigma} \cdot \vec{p}$ -type spin-orbit (SO) coupling. The topology of condensate wavefunctions manifests in the quaternionic representation. The spatial distributions of the  $S^3$  quaternionic phase exhibit 3D skyrmion configurations, while those of the  $S^2$  spin orientation possess non-zero Hopf invariants. As increasing SO coupling strength, spin textures evolve from concentric distributions to lattice structures at weak interactions. Strong interactions change condensates into spin-polarized plane-wave states, or, superpositions of two plane-waves exhibiting helical spin spirals.

PACS numbers: 03.75.Mn, 03.75.Lm, 03.75.Nt, 67.85.Fg

Quantum wavefunctions are generally complex-valued. However, the ground state many-body wavefunctions of single component bosons are usually positive-definite known as “no-node” theorem [1]. This statement is valid under very general conditions: the non-frustrated kinetic energy (e.g. the Laplacian type), arbitrary single particle potential, and coordinate-dependent interactions. This is a strong constraint, which implies that time-reversal (TR) symmetry cannot be spontaneously broken in conventional Bose-Einstein condensations (BEC), such as superfluid  $^4\text{He}$  and most ground state BECs of ultra-cold alkali bosons [3].

It is exciting to seek unconventional BECs with complex-valued condensate wavefunctions which spontaneously break TR symmetry [4]. The “no-node” theorem does not apply to spinful bosons with spin-orbit (SO) coupling because the kinetic energy is not just a Laplacian but also linearly depends on momentum. It is predicted that such condensates can spontaneously develop half-quantum vortex coexisting with 2D skyrmion-type spin textures [5]. Experimentally, spin textures in SO coupled exciton condensations have recently been observed [6]. The progress of synthetic artificial gauge fields in ultracold atomic gases greatly stimulates the investigation of the above exotic physics [7, 8]. Extensive studies have been performed for bosons with 2D Rashba SO coupling which exhibit various spin structures arising from competitions among SO coupling, interaction, and confining trap energy [5, 9–16].

Quaternions are an extension of complex numbers as the first discovered non-commutative division algebra, which has provided a new formulation of quantum mechanics [17–19]. Can we have unconventional BECs with non-trivial quaternionic condensate wavefunctions? Similarly to complex numbers whose phases span a unit circle, the quaternionic phases span a unit three dimensional sphere  $S^3$ . Spin distributions associated with quaternionic wavefunctions are obtained through the 1st Hopf map  $S^3 \rightarrow S^2$ . In 3D, both condensate wavefunctions and spin distributions can be topological non-trivial due

to the homotopy groups  $\pi_3(S^3) = \pi_3(S^2) = \mathbb{Z}$  [20, 21]. The winding number of  $S^3 \rightarrow S^3$  is the 3D skyrmion number and that of the  $S^3 \rightarrow S^2$  is the Hopf invariant.

Since one quaternion can be viewed as a pair of complex-number, two-component spinor wavefunctions map to single-component quaternion-valued ones. This provides a convenient view point to study its topological properties. In this article, we present 3D condensation wavefunctions with non-trivial topological configurations of quaternionic phases, which are stabilized by the 3D SO coupling of the  $\vec{\sigma} \cdot \vec{p}$ -type. The experimental realization of this SO coupling has been proposed by the authors through atom-light interactions in a combined tripod and tetrapod level system [22] and also by Anderson *et al.* [24]. The condensation wavefunctions exhibit topologically non-trivial configurations as 3D skyrmions, and spin density distributions are also non-trivial with non-zero Hopf invariants. Spatial distributions of the quaternionic phase textures and spin textures are concentric at weak SO couplings, and evolve to lattice structures at strong SO couplings.

We consider a two-component boson system with the 3D spin-orbit (SO) coupling of the  $\vec{\sigma} \cdot \vec{p}$ -type confined in a harmonic trap. The free part of the Hamiltonian is defined as

$$H_0 = \int d^3\vec{r} \psi_\alpha^\dagger \left\{ -\frac{\hbar^2 \vec{\nabla}^2}{2m} + i\hbar\lambda \vec{\sigma}_{\alpha\beta} \cdot (\vec{\nabla}) \right. \\ \left. + \frac{1}{2}m\omega^2 \vec{r}^2 \right\} \psi_\beta, \quad (1)$$

where  $\alpha = \uparrow, \downarrow$  refer to two internal states of bosons;  $\lambda$  is the SO coupling strength with the unit of velocity;  $\omega$  is the trap frequency. At single-particle level, Eq. 1 satisfies the Kramer-type time-reversal (TR) symmetry of  $T = (-i\sigma_2)C$  with the property of  $T^2 = -1$ . However, parity is broken by SO coupling. In the absence of the trap, the good quantum numbers for single particle states are the helicity eigenvalues  $\pm 1$  of  $\vec{\sigma} \cdot \vec{p}/|p|$ . This results in two branches of dispersions  $\epsilon_\pm(\vec{k}) = \frac{\hbar^2}{2m}(k - k_{so})^2$  where  $\hbar k_{so} = m\lambda$ . The lowest single particle energy states lie

in the sphere with radius  $k_{so}$  denoted as the SO sphere. It corresponds to an SO length scale  $l_{so} = 1/k_{so}$  in real space. The harmonic trap has a natural length scale  $l_T = \sqrt{\frac{\hbar}{m\omega}}$ , and thus the dimensionless parameter  $\alpha = l_T k_{so}$  describes the relative SO coupling strength. We assume the contact  $s$ -wave scattering interaction defined as

$$H_{int} = \frac{g_{\alpha\beta}}{2} \int d^3\vec{r} \psi_{\alpha}^{\dagger}(\vec{r}) \psi_{\beta}^{\dagger}(\vec{r}) \psi_{\beta}(\vec{r}) \psi_{\alpha}(\vec{r}), \quad (2)$$

and allow two different interaction parameters, including the intra and inter-component ones defined as  $g_{\uparrow\uparrow} = g_{\downarrow\downarrow} = g$ , and  $g_{\uparrow\downarrow} = cg$ , where  $c$  is a constant.

In the previous study of 2D Rashba SO coupling with harmonic potential [5, 15], the single particle eigenstates are intuitively expressed in momentum representation: the low energy state lies around a ring in momentum space, and the harmonic potential becomes the planar rotor operator on this ring subject to a  $\pi$ -flux, which quantizes the angular momentum  $j_z$  to half integers. Similar picture also applies in 3D [5, 23]. The low energy states are around the SO sphere. In the projected low energy Hilbert space, the eigenvectors read  $\psi_{+}(\vec{k}) = (\cos \frac{\theta_{\vec{k}}}{2}, \sin \frac{\theta_{\vec{k}}}{2} e^{i\phi_{\vec{k}}})^T$ . The harmonic potential is again a rotor Hamiltonian on the SO sphere subject to the Berry gauge connection as  $V_{tp} = \frac{1}{2}m(i\nabla_{\vec{k}} - \vec{A}_{\vec{k}})^2$  with the moment of inertial  $I = M_k k_{so}^2$  and  $M_k = \hbar^2/(m\omega^2)$ .  $\vec{A}_{\vec{k}} = i\langle\psi_{+}(\vec{k})|\nabla_{\vec{k}}|\psi_{+}(\vec{k})\rangle$  is the vector potential of the  $U(1)$  magnetic monopole, which quantizes the angular momentum  $j$  to half-integers. While the radial energy is still quantized in terms of  $\hbar\omega$ , the angular energy dispersion with respect to  $j$  is strongly suppressed at large values of  $\alpha$  as

$$E_{n_r, j, j_z} \approx \left(n_r + \frac{j(j+1)}{2\alpha^2}\right)\hbar\omega + \text{const}, \quad (3)$$

where  $n_r$  is the radial quantum number. As further shown in Ref. [22], in the case  $\alpha \gg 1$ , all the states with the same  $n_r$  but different  $j$  and  $j_z$  are nearly degenerate, thus can be viewed as one 3D Landau level with spherical symmetry but broken parity. If filled with fermions, the system belongs to the  $Z_2$ -class of 3D strong topological insulators.

Now we load the system with bosons. The interaction energy scale is defined as  $E_{int} = gN_0/l_T^3$  where  $N_0$  is the total particle number in the condensate. The corresponding dimensionless parameter is  $\beta = E_{int}/\hbar\omega$ . The Gross-Pitaevskii (GP) equation at the Hartree-Fock level (HF) is obtained as

$$E \begin{pmatrix} \psi_{\uparrow} \\ \psi_{\downarrow} \end{pmatrix} = \left\{ -\frac{\hbar^2 \nabla^2}{2m} - i\lambda \hbar \vec{\nabla} \cdot \vec{\sigma}_{\alpha\beta} + \frac{1}{2}m\omega^2 r^2 + g \begin{pmatrix} n_{\uparrow} + cn_{\downarrow} & 0 \\ 0 & cn_{\uparrow} + n_{\downarrow} \end{pmatrix} \right\} \begin{pmatrix} \psi_{\uparrow} \\ \psi_{\downarrow} \end{pmatrix}, \quad (4)$$

where  $n_{\uparrow, \downarrow}(\vec{r}) = N_0 |\psi_{\uparrow, \downarrow}(\vec{r})|^2$  are the particle densities of two components, respectively. Eq. 4 is solved numerically by using imaginary time evolution.

We first consider the limit of weak SO coupling, say,  $\alpha \sim 1$  and weak interactions. In this case, the gap between single particle energy levels is large. The condensate wavefunction  $\psi$  remains the same symmetry structure as the single particle one over a wide range of interaction parameter  $\beta$ , i.e.,  $\psi$  remains the eigenstates of  $j = \frac{1}{2}$  as confirmed numerically.  $\psi$  can be represented as

$$\psi_{j=j_z=\frac{1}{2}}(r, \hat{\Omega}) = f(r)Y_{\frac{1}{2}, 0, \frac{1}{2}}^{+}(\hat{\Omega}) + ig(r)Y_{\frac{1}{2}, 1, \frac{1}{2}}^{-}(\hat{\Omega}), \quad (5)$$

where  $f(r)$  and  $g(r)$  are real radial functions.  $Y_{j, l, j_z}^{\pm}$  are defined as the SO coupled spherical harmonics with  $j = l \pm 1/2$  with the parity eigenvalues  $(-)^l$ , respectively. For example,  $Y_{\frac{1}{2}, 0, \frac{1}{2}}^{+}(\hat{\Omega}) = (1, 0)^T$ , and  $Y_{\frac{1}{2}, 1, \frac{1}{2}}^{-}(\hat{\Omega}) = (\cos \theta, \sin \theta e^{i\phi})^T$ . The TR partner of Eq. 5 is  $\psi_{j_z=-\frac{1}{2}} = \hat{T}\psi_{j=j_z=\frac{1}{2}}$ . The two terms in Eq. 5 are of opposite parity eigenvalues, mixed by the parity breaking  $\vec{\sigma} \cdot \vec{p}$  term. The coefficient of  $i$  of the  $Y_{jj_z}^{-}$  term is because the matrix element  $\langle Y_{jj_z}^{+} | \vec{\sigma} \cdot \vec{p} | Y_{jj_z}^{-} \rangle$  is purely imaginary. For the non-interacting case, the radial wavefunctions up to a Gaussian factor can be approximated by spherical Bessel functions as  $f(r) \approx j_0(k_{so}r)e^{-r^2/2l_T^2}$  and  $g(r) \approx j_1(k_{so}r)e^{-r^2/2l_T^2}$ , which correspond to  $s$  and  $p$  partial waves, respectively. Both of them exhibit the pitch value around  $k_{so}$ . At  $r = 0$ ,  $f(r)$  is at maximum and  $g(r)$  is 0. As  $r$  increases, roughly speaking, the zero points of  $f(r)$  corresponds to the extrema of  $g(r)$  and vice versa. Repulsive interactions expand the spatial distributions of  $f(r)$  and  $g(r)$ , but the above picture still holds qualitatively. In other words, there is a  $\frac{\pi}{2}$ -phase shift between the oscillations of  $f(r)$  and  $g(r)$ .

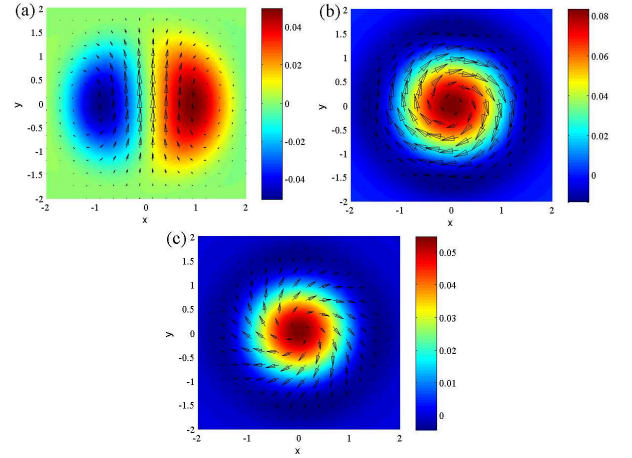


FIG. 1: The distribution of  $\vec{S}(\vec{r})$  in a) the  $xz$ -plane and in the horizontal planes with b)  $z = 0$  and c)  $z/l_T = \frac{1}{2}$ . The color scale shows the magnitude of out-plane component  $S_y$  in a) and  $S_z$  in b) and c). The parameter values are  $\alpha = 1.5$ ,  $c = 1$ , and  $\beta = 30$ , and the length unit in these and all the figures below is  $l_T$ .

The topological structure of condensate wavefunction Eq. 5 manifests clearly in the quaternion representation.

The complex two-component vector  $\psi = (\psi_\uparrow, \psi_\downarrow)^T$  can be mapped to a quaternion variable through  $\xi = \xi_0 + \xi_1 i + \xi_2 j + \xi_3 k$ , where  $\xi_0 = \text{Re}\psi_\uparrow$ ,  $\xi_1 = \text{Im}\psi_\downarrow$ ,  $\xi_2 = -\text{Re}\psi_\downarrow$ ,  $\xi_3 = \text{Im}\psi_\uparrow$ ;  $i, j, k$  are the imaginary units satisfying  $i^2 = j^2 = k^2 = -1$ , and the anti-commutation relation  $ij = -ji = k$ . The TR transformation on  $\xi$  is just  $-\bar{j}\xi$ . Eq. 5 can be expressed in the quaternionic exponential form as

$$\xi_{j=z=\frac{1}{2}}(r, \hat{\Omega}) = |\xi(r)|e^{\vec{\omega}(\hat{\Omega})\gamma(r)} = |\xi|(\cos \gamma + \vec{\omega} \sin \gamma), \quad (6)$$

where  $|\xi(r)| = [f^2(r) + g^2(r)]^{\frac{1}{2}}$ ,  $\cos \gamma(r) = f(r)/|\xi(r)|$ , and  $\sin \gamma(r) = g(r)/|\xi(r)|$ .  $\vec{\omega}(\hat{\Omega}) = \sin \theta \cos \phi i + \sin \theta \sin \phi j + \cos \theta k$ , which is the imaginary unit along the direction of  $\hat{\Omega}$ , and satisfies  $\vec{\omega}^2(\hat{\Omega}) = -1$ . According to the oscillating properties of  $f(r)$  and  $g(r)$ ,  $\gamma(r)$  spirals as  $r$  increases. At the  $n$ -th zero point of  $g(r)$  denoted  $r_n$ ,  $\gamma(r_n) = n\pi$  ( $n \geq 0$  and we define  $r_0 = 0$ ), while at the  $n$ -th zero point of  $f(r)$  denoted  $r'_n$ ,  $\gamma(r'_n) = (n - \frac{1}{2})\pi$  ( $n \geq 1$ ).

The spatial distribution of the quaternionic phase  $e^{\vec{\omega}(\hat{\Omega})\gamma(r)}$  defined in Eq. 6, which lies on  $S^3$ , exhibits a topologically nontrivial mapping from  $R^3$  to  $S^3$ , i.e., a 3D multiple skyrmion configuration. This type of topological defects are non-singular which is different from the usual vortex in single component BEC. For a closed 3-manifold, the Pontryagin index  $\pi_3(S^3) = Z$ . However, the coordinate space is the open  $R^3$ . At large distance  $r \gg l_T$ ,  $|\xi(r)|$  decays exponentially. The quaternionic phase and the mapping are not well-defined. Nevertheless, in each concentric spherical shell with  $r_n < r < r_{n+1}$  denoted as  $Sh_n$ ,  $\gamma(r)$  winds from  $n\pi$  to  $(n+1)\pi$ , and  $\vec{\omega}(\hat{\Omega})$  covers all the directions, thus  $Sh_n$  contributes 1 to the winding number of  $e^{\vec{\omega}(\hat{\Omega})\gamma(r)}$  on  $S^3$ . If the system size is truncated at the order of  $l_T$ , the skyrmion number can be approximated at the order of  $l_T k_{so} = \alpha$ . In the previously studied 2D case, the spin density distribution exhibit 2D skyrmion configuration due to  $\pi_2(S^2)$  [5, 15, 16], while condensation wavefunctions have no well-defined topology due to  $\pi_2(S^3) = 0$ .

Exotic spin textures in spinor condensates have been extensively investigated [25–27]. In our case, the 3D spin density distributions  $\vec{S}(\vec{r})$  exhibit a novel configuration with non-trivial Hopf invariants.  $\vec{S}(\vec{r})$  can be obtained from  $\xi(r)$  through the 1st Hopf map defined as  $\vec{S}(\vec{r}) = \frac{1}{2}\psi^\dagger_\alpha \vec{\sigma}_{\alpha\beta} \psi_\beta$ , or in the quaternionic representation,

$$\frac{1}{2}\bar{\xi}k\xi = S_x i + S_y j + S_z k \quad (7)$$

where  $\bar{\xi} = \xi_0 - \xi_1 i - \xi_2 j - \xi_3 k$  is the quaternionic conjugate of  $\xi$ . The homotopy group from  $S^3$  to  $S^2$  is  $\pi_3(S^2) = Z$  characterized by the integer valued Hopf invariant. The Hopf invariant of the 1st Hopf map is just 1 [21]. The real space concentric spheric shell  $Sh_n$  maps to the quaternionic phase  $S^3$ , and the latter further maps to the  $S^2$  Bloch sphere through the 1st Hopf map. The winding

number of the first map is 1, and the Hopf invariant of the second map is also 1, thus the Hopf invariant of the  $Sh_n$  to  $S^2$  is 1. Rigorously speaking, the magnitude of  $\vec{S}(\vec{r})$  decays exponentially at  $r \gg l_T$ , and thus the total Hopf invariant is not well-defined in the open  $R^3$  space. Again, if we truncate the system size at  $l_T$ , the Hopf invariant is approximately at the order of  $\alpha$ .

Next we present numeric results for the spin textures associated with the condensation wavefunction Eq. 5 as plotted in Fig. 1. Explicitly,  $\vec{S}(\vec{r})$  is expressed as

$$\begin{aligned} \begin{bmatrix} S_x(\vec{r}) \\ S_y(\vec{r}) \end{bmatrix} &= g(r) \sin \theta \begin{bmatrix} \cos \phi & -\sin \phi \\ \sin \phi & \cos \phi \end{bmatrix} \begin{bmatrix} g(r) \cos \theta \\ f(r) \end{bmatrix}, \\ S_z(\vec{r}) &= f^2(r) + g^2(r) \cos 2\theta, \end{aligned} \quad (8)$$

In the  $xz$ -plane, the in-plane components  $S_x$  and  $S_z$  form a vortex in the half plane of  $x > 0$  and  $S_y$  is prominent in the core. The contribution at large distance is neglected, where  $\vec{S}(\vec{r})$  decays exponentially. Due to the axial symmetry of  $\vec{S}(\vec{r})$  in Eq. 8, the 3D distribution is just a rotation of that in Fig. 1 a) around the  $z$ -axis. In the  $xy$ -plane, spin distribution exhibits a 2D skyrmion pattern, whose in-plane components are along the tangential direction. As the horizontal cross-section shifted along the  $z$ -axis,  $\vec{S}(\vec{r})$  remains 2D skyrmion-like, but its in-plane components are twisted around the  $z$ -axis. The spin configuration at  $z = -z_0$  can be obtained by a combined operation of TR and rotation around the  $y$ -axis  $180^\circ$ , thus its in-plane components are twisted in an opposite way compared to those at  $z = z_0$ . Combining the configurations on the vertical and horizontal cross sections, we complete the 3D distribution of  $\vec{S}(\vec{r})$  with non-zero Hopf invariant.

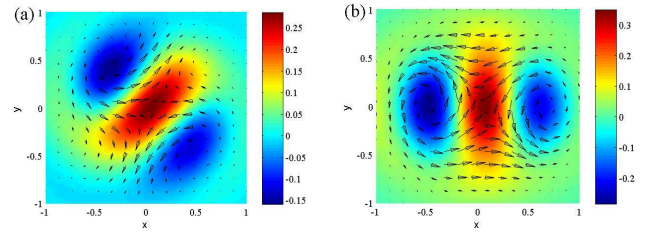


FIG. 2: The distribution of  $\vec{S}(\vec{r})$  in horizontal cross-sections with a)  $z/l_T = -0.5$ , b)  $z/l_T = 0$ , respectively. The color scale shows the value of  $S_z$ , and parameter values are  $\alpha = 4$ ,  $\beta = 2$ , and  $c = 1$ .

Next we consider the case of intermediate SO coupling strength, which suppresses the gap between the lowest and the second single particle levels. Interactions mix single-particle eigenstates with different values of  $j$ , such that rotational symmetry is broken and complex patterns appear. In this case, the topology of condensate wavefunctions is still 3D skyrmion-like mapping from  $R^3$  to  $S^3$ , and spin textures with the non-trivial Hopf invariant are obtained through the 1st Hopf map. Compared to

the weak SO coupling case, quaternionic phase skyrmions and spin textures are no longer concentric, but split to a multi-centered pattern. The numeric results of  $\vec{S}(\vec{r})$  are plotted in Fig. 2 for horizontal cross-sections. In the  $xy$ -plane,  $\vec{S}$  exhibits the 2D skyrmion pattern: the in-plane components form two vortices and one anti-vortex, while  $S_z$ 's inside the vortex and anti-vortex cores are opposite in direction, thus they contribute to the skyrmion number with the same sign. The spin configuration at  $z = z_0 > 0$  is shown in Fig. 2 (b), which is twisted around the  $z$ -axis clock-wise. After performing the combined TR and rotation around the  $y$ -axis  $180^\circ$ , we arrive at the configuration at  $z = -z_0$ .

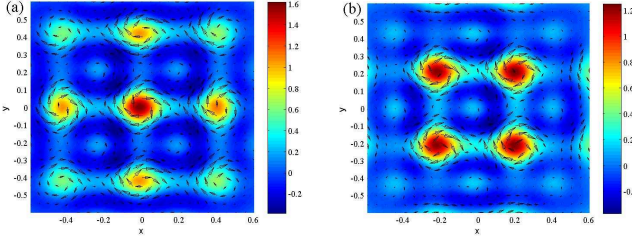


FIG. 3: The distribution of  $\vec{S}(\vec{r})$  in horizontal cross-sections with (a)  $z/l_T = 0$ , (b)  $z/l_T = 0.2$ , respectively. The color scale shows the value of  $S_z$  and parameter values are  $\alpha = 15$ ,  $\beta = 0.8$ , and  $c = 1$ . The overall lattice exhibits the bcc structure.

Next we consider the case of strong SO coupling, i.e.,  $\alpha \gg 1$ . The single-particle eigenstates with  $n_r = 0$  are nearly degenerate i.e., they are the lowest Landau level (LLL) states. We assume interactions weak enough to neglect the inter-Landau level mixing but still relatively strong to mix different states inside the LLL. Lattice structures are formed, and each site is a single 3D skyrmion for the condensate wavefunction  $\xi(\vec{r})$ , which corresponds to a spin texture with approximately a unit Hopf invariant. The numeric results for the spin texture configuration are depicted in Fig. 3 a) and b). In the  $xy$ -plane, the spin textures form a square lattice, and the lattice constant  $d$  is related to the SO length scale  $d \simeq 2\pi l_{so} = 2\pi l_T/\alpha$ . For the horizontal cross-section  $z \simeq d/2$ , spin textures also form a square lattice whose sites sit above the plaquette centers of the former lattice. Similar structure also occurs at  $z \simeq -d/2$ . Thus the topological defects form a body-centered cubic (bcc) lattice even though its size is finite confined by the trap.

If in the strong SO coupling case, interactions are also strong to mix different Landau levels, we can neglect the effect of the harmonic trapping potential. The condensate wavefunctions select plane-wave states located on the SO sphere and are no longer topological. At  $c = 1$ , the interaction is spin-independent, and bosons select a superposition of a pair of states  $\pm \vec{k}$  on the SO sphere, say,  $\pm k_{so} \hat{z}$ . The condensate wavefunction is written as

$$\psi(\vec{r}) = \sqrt{N_a/N_0} e^{ik_{so}z} |\uparrow\rangle + \sqrt{N_b/N_0} e^{-ik_{so}z} |\downarrow\rangle, \quad (9)$$

with  $N_a + N_b = N_0$ . The density of Eq. 9 in real space is uniform to minimize the interaction energy at the Hartree-Fock level. However, all the different partitions of  $N_{a,b}$  yield the same Hartree-Fock energy. The quantum zero point energy from the Bogoliubov modes removes this accidental degeneracy through the “order from disorder” mechanism, which selects the equal partition  $N_a = N_b$ . The calculation is in parallel to that of the 2D Rashba case performed in Ref. [5], thus will not be presented here. In this case, the condensate is a spin helix propagates along  $z$ -axis and spin spirals in the  $xy$ -plane. At  $c \neq 1$ , the spin-dependent part of the interaction can be written as  $H_{sp} = \frac{1-c}{2} g \int d^3r (\psi^\dagger_\uparrow \psi_\uparrow - \psi^\dagger_\downarrow \psi_\downarrow)^2$ . At  $c > 1$ , the interaction energy at Hartree-Fock level is minimized for the condensate wavefunction of a plane wave state  $e^{ik_{so}z} |\uparrow\rangle$ , or, its TR partner. For  $c < 1$ ,  $\langle H_{sp} \rangle$  is minimized if  $\langle S_z \rangle = 0$  in space. At the HF level, the condensate can either be a plane-wave state in the equator of the SO sphere with spin polarizing in the  $xy$ -plane, or, the spin spiral state of Eq. 9 with  $N_a = N_b$ . An “order from disorder” analysis on the Bogoliubov zero point energies indicates that the spin spiral state is selected. We also present the numerical results for Eq. 4 with a harmonic trap in Fig. 4 for the case of  $c < 1$ . The condensate momenta of two spin components have opposite sign, thus the trap inhomogeneity already prefers the spin spiral state Eq. 9 at the HF level.

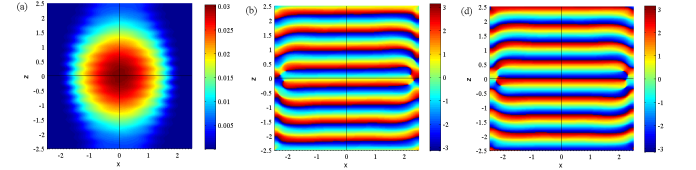


FIG. 4: The density profile (a) for  $\uparrow$ -component, and that for  $\downarrow$ -component is the same. Phase profiles for (b)  $\uparrow$  and (c)  $\downarrow$ - components, respectively. Parameter values are  $a = 10$ ,  $g = 50$ , and  $c = 0.5$ .

To summarize, we have investigated the two-component unconventional BECs driven by the 3D SO coupling. In the quaternionic representation, the quaternionic phase distributions exhibit non-trivial 3D skyrmion configurations from  $R^3$  to  $S^3$ . The spin orientation distributions exhibit texture configurations characterized by non-zero Hopf invariants from  $R^3$  to  $S^2$ . These two topological structures are connected through the 1st Hopf map from  $S^3$  to  $S^2$ . At large SO coupling strength, the crystalline order of spin textures, or, wavefunction skyrmions, are formed, which can be viewed as a generalization of the Abrikosov lattice in 3D.

*Note added* Near the completion of this manuscript, we became aware of a related work by Kawakami *et al.* [28], in which the condensate wavefunction in the weak SO coupling case was studied.

X. F. Z. gratefully acknowledges the support of NFRP (2011CB921204, 2011CBA00200), NNSF

(60921091), NSFC (11004186), and CUSF, SRFDP (20103402120031), and the China Postdoctoral Science Foundation. Y. L. and C. W. are supported by AFOSR YIP program and NSF-DMR-1105945.

- 
- [1] R. P. Feynman, *Statistical Mechanics, A Set of Lectures* (Berlin: Addison-Wesley, 1972).
  - [2] R. B. Bapat and T. Raghavan, *Non-Negative Matrices and Applications* (Cambridge University Press, Cambridge, United Kingdom, 1997).
  - [3] A. J. Leggett, Rev. Mod. Phys. **73**, 307 (2001).
  - [4] C. Wu, Mod. Phys. Lett. **23**, 1 (2009).
  - [5] C. Wu, I. Mondragon-Shem, arXiv:0809.3532; C. Wu, I. Mondragon-Shem, and X. F. Zhou, Chin. Phys. Lett., **28**, 097102 (2011).
  - [6] A.A. High *et al.*, Nature **483**, 584 (2012). A.A. High *et al.*, arXiv:1103.0321.
  - [7] Y.-J. Lin *et al.*, Nature **462**, 628 (2009).
  - [8] Y.-J. Lin, K. Jiménez-García and I. B. Spielman, Nature **471**, 83 (2011).
  - [9] T. Stanescu, B. Anderson, V. Galitski Phys. Rev. A **78**, 023616 (2008).
  - [10] T.-L. Ho and S. Zhang, Phys. Rev. Lett. **107**, 150403 (2011).
  - [11] C. Wang, C. Gao, C.M. Jian, H. Zhai, Phys. Rev. Lett. **105**, 160403 (2010).
  - [12] S.-K. Yip, Phys. Rev. A **83**, 043616 (2011).
  - [13] Y. Zhang, L. Mao, and C. Zhang, Phys. Rev. Lett. **108**, 035302 (2012).
  - [14] X.-F. Zhou, J. Zhou, and C. Wu, Phys. Rev. A **84**, 063624 (2011).
  - [15] H. Hu, B. Ramachandhran, H. Pu, and X.J Liu, Phys. Rev. Lett. **108**, 010402(2012).
  - [16] S. Sinha, R. Nath, and L. Santos, arXiv:1102.2045.
  - [17] A. V. Balatsky, cond-mat/9205006.
  - [18] S. L. Adler, *Quaternionic Quantum Mechanics and Quantum Fields* (Oxford University Press, Oxford, 1995).
  - [19] D. Finkelstein *et al.*, J. Math. Phys. (N. Y.) **3**, 207 (1962).
  - [20] F. Wilczek and A. Zee, Phys. Rev. Lett. **51**, 2250 (1983).
  - [21] M. Nakahara, *Geometry, topology, and physics*, (Taylor & Francis, 2003)
  - [22] Y. Li, X. Zhou, and C. Wu, Phys. Rev. B **85**, 125122 (2012).
  - [23] S.K. Ghosh, J.P. Vyasankere, V.B. Shenoy, Phys. Rev. A, **84**, 053629 (2011).
  - [24] B. M. Anderson, G. Juzeliunas, I. B. Spielman, V. M. Galitski, arXiv:1112.6022.
  - [25] F. Zhou, Int. J. Mod. Phys. B **17**, 2643-2698(2003); E. Demler and F. Zhou, Phys. Rev. Lett. **88**, 163001(2002). G. W. Semenoff and F. Zhou, Phys. Rev. Lett. **98**, 100401 (2007).
  - [26] J. Zhang and T. L. Ho, arXiv:0908.1593.
  - [27] D. M. Stamper-Kurn, and M. Ueda, arXiv:1205.1888.
  - [28] T. Kawakami *et al.*, arXiv:1204.3177.